Wave energy converter array layout control co-design for different mooring configurations

Yerai Peña-Sanchez, Demián García-Violini, Ander Zarketa, Markel Penalba, Vincenzo Nava, and John V. Ringwood

Abstract—**This paper introduces a comprehensive control co-design (CCD) methodology for optimising the layout of wave energy converter (WEC) arrays from an economic perspective. The CCD approach ensures that all optimised WEC and array parameters are aligned with the final control strategy, resulting in an optimal design from an overall perspective. By integrating a spectral-based control strategy into the array layout design, this study aims to achieve an optimal WEC array layout that maximises energy absorption while considering the economic cost of the system. The proposed methodology provides a unique design approach that combines optimal layout design with optimal control performance. The analysis focuses on a three-device in-line WEC array, with different spacing and mooring arrangements. Energy capture and system cost evaluation are calculated, and the results obtained using the spectral-based controller are compared with those obtained using a benchmark passive controller. The findings underscore the importance of integrating advanced control strategies at the design stage to enhance energy absorption and cost reduction.**

Index Terms—**Wave Energy, Control co-design, Hydrodynamic coefficients, Interpolation, Extrapolation**

I. Introduction

Ocean waves possess a substantial reservoir of untapped energy potential, positioning them as a potential significant contributor to transforming the existing global energy mix. The wave energy community has explored various wave energy converter (WEC) prototypes that utilize different principles of energy absorption. Even though some of these prototypes have shown technical feasibility, none have achieved economic viability yet, indicating their unpreparedness to compete with other energy sources in the market.

To improve the economic viability of wave energy converters (WECs), two primary actions have been identified. Firstly, deploying WECs in large arrays and optimizing their layout and subsystems can help reduce costs, including both initial investment (CapEx) and ongoing operational expenses (OpEx). Secondly, enhancing the energy absorption capabilities of these devices requires the development of advanced control strategies focused on maximizing energy extraction. Therefore, from an economic standpoint, it is crucial to design more reliable prototypes that optimize key aspects of WECs and WEC arrays, such as array layout, floater shape, power take-off (PTO) system, and mooring lines. However, it is important to emphasize that these optimizations should be performed considering control conditions, as they play a significant role in cost reduction.

Traditionally, the optimization process involves considering energy absorption capabilities and loading on critical elements, while the PTO is driven by simplified control strategies (such as passive resistive control approaches). Advanced control strategies are then developed to maximize energy extraction while maintaining the system physical integrity through active constraint handling mechanisms [1]. However, this optimization process does not guarantee that all aspects of the WECs or WEC arrays are optimal when considering the final control strategy, since the implementation of advanced control strategies significantly alters the WEC motion. The mismatch between the behaviour of the (optimised) WEC design and the behaviour when considering advanced control is addressed by applying design constraints to the controller, which may lead to sub-optimal results [2].

To address such a challenge, control co-design (CCD) of WECs or WEC arrays [3], where optimisation is carried out considering the final control strategy, has gained popularity as a more integrative approach. In other words, this design paradigm emphasizes an optimization approach that is *control-aware*. Several studies in the literature have demonstrated the benefits of CCD for the optimisation of different WEC-related parameters. For example, [3] highlights that CCD strategies contribute significantly to achieving an optimal

Yerai Peña-Sanchez is funded by the European Union's Horizon 2020 research and innovation programme under the Marie Sklodowska-Curie grant agreements N°101034297.

Demián García-Violini is supported by the Agencia I+D+i from the Government of Argentina under grant PICT-2021-I-INVI-00190.

Markel Penalba and Ander Zarketa-Astigarraga are funded by *MCIN/AEI/10.13039/501100011033 ERDF A way of making Europe* under the Grant PID2021-124245OA-I00 and by the Basque Government's ELKARTEK 2022 program under Grant KK-2022/00090.

John Ringwood is supported by Science Foundation Ireland (SFI) through the MaREI Centre for Energy, Climate and Marine under Grant No. 12/RC/2302_P2.

Yerai Peña-Sanchez is with Euskal Herriko Unibertsitatea (EHU/UPV), Bizcaia, Spain (e-mail: yerai.pena@ehu.eus, corresponding author).

Demián García-Violini is with Departamento de Ciencia y Tecnología, Universidad Nacional de Quilmes, Roque Saenz Peña 352, Bernal B1876, Argentina, Consejo Nacional de Investigaciones Científicas y Técnicas (CONICET), Argentina, and Center for Ocean Energy Research, Maynooth University, Maynooth, Ireland.

Ander Zarketa and Markel Penalba are with Fluid Mechanics, Mondragon University, Loramendi 4, Arrasate, Spain. Markel Penalba is also with Ikerbasque, Basque Foundation for Science, Euskadi Plaza 5, Bilbao, Spain.

Vincenzo Nava is with the Basque Center for Applied Mathematics (BCAM), Mazarredo Zumarkalea 14, Bilbao, Spain, and Tecnalia-BRTA, Astondo Bidea 700, Derio, Spain.

John V. Ringwood is with Center for Ocean Energy Research, Maynooth University, Maynooth, Ireland.

Digital Object Identifier:
https://doi.org/10.36688/ewtec-2023-531

structural design for the absorber geometry, aligning it with the energy-maximizing control scheme. Another interesting example is [4], where the authors optimize the PTO configuration considering a spectral-control technique [5]. Finally, from a WEC array perspective, [6] highlights the significance of employing different control techniques to optimize the layout of the WEC array. The study in [6] emphasizes that the behaviour of individual WECs under different control techniques can greatly influence the expected interaction between devices, potentially shifting interaction from destructive to constructive. This has a substantial impact on the overall performance of the array, underscoring the importance of carefully considering the control strategy in WEC array design.

In this paper, a comprehensive CCD methodology is proposed to optimize the layout of a WEC array *from an economic perspective*. The study incorporates a multiple-input multiple-output (MIMO) spectral control technique and explores various mooring configurations. The analysis focuses on a three-device in-line array, where the inter-device distances are independently adjusted, each associated with a distinct mooring configuration. By evaluating the energy capture and system cost for each layout configuration (assuming consistent WECs and subsystems costs and, hence, only varying the mooring system cost), and comparing the results with those obtained using a passive controller, the study underscores the significance of integrating an advanced control strategy at the design stage.

The subsequent sections of this paper are structured as follows. Section II provides a recap of the fundamental principles involved in WEC array modeling. The spectral-based control scheme, to maximize energy absorption while adhering to specified physical constraints, is introduced in Section III. Section IV outlines the CCD methodology for optimizing the layout of WEC arrays, emphasizing the considerations necessary to achieve an array scheme that aligns with the energy-maximizing control scheme. To demonstrate the effectiveness of the proposed approach, an illustrative example featuring a realistic, full-scale WEC array system, is presented in Section V. Finally, Section VI concludes this study by summarizing the key findings and discussing the implications of the presented approach.

II. WEC ARRAY MODELLING

A dynamic model of the WEC array system is established by considering the interaction between the fluid (water) and the floating bodies, and it takes into account the interactions between the different bodies resulting from the radiated and diffracted waves from the devices in the vicinity. It should be noted that, without loss of generality, single-degree-of-freedom (DoF) WECs are considered in this study, in order to simplify the problem. Thus, the formulation of the model can be described, in the time-domain, based on Newton's second law as

$$(m+\mu_\infty)\,\ddot{x}(t) = f_\mathrm{e}(t) - f_\mathrm{h}(t) - f_\mathrm{r}(t) - f_\mathrm{m}(t) - f_\mathrm{u}(t), \quad (1)$$

where $m \in \mathbb{R}^{n_\mathrm{b}\times n_\mathrm{b}}$ is the mass matrix containing the mass of each device in the diagonal and zeros elsewhere, n_b the number of bodies composing the array, $\mu_\infty \in \mathbb{R}^{n_\mathrm{b}\times n_\mathrm{b}}$ the infinite frequency added mass of the WECs (in the diagonal) and the interactions (in the off-diagonal), and $x(t) \in \mathbb{R}^{n_\mathrm{b}}$, $\dot{x}(t) \in \mathbb{R}^{n_\mathrm{b}}$, or equivalently $v(t)$, and $\ddot{x}(t) \in \mathbb{R}^{n_\mathrm{b}}$, or equivalently $a(t)$, are vectors containing the position, velocity and acceleration of the WECs. The forces acting on the WECs (introduced in Equation (1)) are the hydrostatic force $f_\mathrm{r}(t) = S_\mathrm{h}x(t)$ arising due to buoyancy and gravity forces, with $s_\mathrm{h} \in \mathbb{R}^{n_\mathrm{b}\times n_\mathrm{b}}$ the hydrostatic stiffness matrix; the radiation force arising from the waves radiated by the motion of the WECs is defined using the convolution integral as $f_\mathrm{r}(t) = k_{\mathrm{r}_{i,j}}(t) * \dot{x}_j(t)$, with $k_\mathrm{r}(t)$ the radiation convolution kernel; the mooring force which, in this case, is modelled using a spring-damper system as $f_\mathrm{m}(t) = k_\mathrm{m}x(t) + b_\mathrm{m}\dot{x}(t)$, with $k_\mathrm{m} \in \mathbb{R}^{n_\mathrm{b}\times n_\mathrm{b}}$ and $b_\mathrm{m} \in \mathbb{R}^{n_\mathrm{b}\times n_\mathrm{b}}$ the mooring stiffness and damping matrices; and the wave excitation and PTO control forces are defined as $f_\mathrm{e}(t) \in \mathbb{R}^{n_\mathrm{b}}$ and $f_\mathrm{u}(t) \in \mathbb{R}^{n_\mathrm{b}}$, respectively.

Note that both the infinite frequency added mass matrix (μ_∞) and the radiation convolution kernel matrix (k_r) can be computed from the frequency-domain radiation added-mass and damping ($A_\mathrm{r}(\omega) \in \mathbb{R}^{n_\mathrm{b}\times n_\mathrm{b}}$ and $B_\mathrm{r}(\omega) \in \mathbb{R}^{n_\mathrm{b}\times n_\mathrm{b}}$ hydrodynamic coefficients, respectively) following Ogilvie's relations [7] as

$$\begin{aligned} A_\mathrm{r}(\omega) &= \mu_\infty - \tfrac{1}{\omega}\int_0^{+\infty} k_\mathrm{r}(t)\sin(\omega t)dt, \\ B_\mathrm{r}(\omega) &= \int_0^{+\infty} k_\mathrm{r}(t)\cos(\omega t)dt. \end{aligned} \quad (2)$$

Analogously, the radiation convolution kernel can be defined, in the frequency-domain[1], as

$$K_\mathrm{r}(\omega) = B_\mathrm{r}(\omega) + \jmath\omega\left[A_\mathrm{r}(\omega) - \mu_\infty\right]. \quad (3)$$

Thus, it is possible now to define Equation (1) in the frequency-domain, by means of the force-to-velocity description of the array [8], as

$$V(\omega) = Z_i^{-1}(\omega)\left[F_\mathrm{e}(\omega) - F_\mathrm{u}(\omega)\right], \quad (4)$$

with $Z_i(\omega) \in \mathbb{I}^{n_\mathrm{b}\times n_\mathrm{b}}$, the intrinsic system impedance, defined as

$$Z_i(\omega) = B_\mathrm{r}(\omega) + b_\mathrm{m} + \jmath\omega\left(m + A_\mathrm{r}(\omega) - \frac{s_\mathrm{h}+s_\mathrm{m}}{\omega^2}\right). \quad (5)$$

It is possible now to define the force-to-velocity transfer function [9], which is a requirement for control design purposes, from Equation (5), as

$$G_\mathrm{fv}(\omega) = \jmath\omega\left[-\omega^2(m+\mu_\infty) + \jmath\omega(H_\mathrm{r}(\omega) + b_\mathrm{m}) + s_\mathrm{h} + s_\mathrm{m}\right]^{-1}, \quad (6)$$

In Eq. (6), the calculation of $H_\mathrm{r}(\omega)$ typically involves the use of boundary-element methods like NEMOH [10]. However, for various applications, such as control, it is often more convenient to work with an approximate representation $\hat{H}_\mathrm{r}(s)|_{s=j\omega} \approx H_\mathrm{r}(\omega)$, where $s = \jmath\omega$ and $\hat{H}_\mathrm{r}(s)$ is a stable linear time-invariant (LTI) system. This approximation is commonly utilized in the literature [9], and its determination can be facilitated

[1]Note that using capital letters on the name of a (lower-case) variable denotes the frequency-domain analogous of such variable.

by employing advanced system identification software, such as the FOAMM toolbox [11]. By adopting an LTI system approximation for the radiation kernel, the system presented in Equation (6) can be reformulated as a unified (MIMO) transfer function matrix or, alternatively, represented in state-space form.

Finally, it should be noted that the required frequency-domain hydrodynamic parameters $A_{\mathrm{r}}(\omega)$ and $B_{\mathrm{r}}(\omega)$, in addition to the excitation force parameters required to define the mapping from wave elevation to excitation force ($\mathcal{H}_{\mathrm{e}}(\omega)$), can be computed using boundary element method (BEM) solvers such as, for example, NEMOH [10] or WAMIT [12].

III. Spectral Control Approach

This section provides an overview of the spectral control strategy employed in this study. In general, spectral controllers are control schemes that optimize the control input by solving an optimization problem, based on a direct transcription method which represents the system variables using a suitable set of basis functions. They are capable of handling physical constraints and, in theory, achieve optimal solutions [13] (according to the considered basis function resolution). In the context of this study, a spectral-based controller is used to ensure optimal power capture while considering realistic motion and PTO force ranges, by including position and control force constraints. In Sections III-A and III-B, the general control objective in WECs and the fundamental principles of spectral controllers are discussed, respectively.

A. Control objective

The primary objective in a WEC control problem is to maximize the total absorbed energy. In a WEC system, which experiences an external excitation force $f_{\mathrm{e}}(t)$ and is controlled through a PTO force $f_{\mathrm{u}}(t)$, the total absorbed energy by all the devices in the array ($E \in \mathbb{R}$) during the time interval $[0, T]$ can be calculated as

$$E = -\int_0^T P(t)dt = -\int_0^T \dot{x}^{\intercal}(t) f_{\mathrm{u}}(t)dt, \tag{7}$$

with $P(t) \in \mathbb{R}$ as the instantaneous absorbed power. Therefore, the control problem is usually defined as

$$\begin{aligned} \max_{f_{\mathrm{u}}(t)} \quad & -\int_0^T \dot{x}(t)^{\intercal} f_{\mathrm{u}}(t)dt \\ \text{subject to} \quad & \begin{cases} \dot{\mathrm{x}} = \mathcal{F}(\mathrm{x}, f_{\mathrm{u}}, f_{\mathrm{e}}) \\ \dot{x} = \mathcal{G}(\mathrm{x}) \\ \mathcal{C} \end{cases} \end{aligned} \tag{8}$$

where $\mathcal{F}(x, f_{\mathrm{u}}, f_{\mathrm{e}})$ represents the MIMO state-space system of the WEC (obtained from Equation (1)), $\mathcal{G}(\mathrm{x})$ the output mapping of the state space as $\mathrm{x} \mapsto \dot{x}$, and $\mathcal{C}$ the set of considered constraints which, in this case, solely considers displacement and PTO force constraints ($x_{\min} \leq x(t) \leq x_{\max}$ and $f_{\min} \leq f_{\mathrm{u}}(t) \leq f_{\max}$, respectively).

B. Spectral approximation & control

In this paper, we explore a control methodology that relies on (pseudo-)spectral techniques to address the control problem presented in Equation (8). The first step involves discretising the optimal control formulation from Equation (8) in the spectral domain. This is accomplished by projecting the state vector $x(t)$ and the control force $\mathrm{f_u}$ onto an orthonormal vector space of dimension N, using a linear combination of orthogonal basis functions denoted as $\Phi = [\phi_1, \phi_2, \cdots, \phi_N]$. One possible choice for the basis functions is the Fourier basis, inspired by the harmonic nature of the WEC variables. As a result, the states and control force can be approximated as

$$\mathrm{x}(t) \approx \mathrm{x}^N(t) = \hat{\mathrm{x}}\Phi(t)^{\intercal}, \text{ and } \quad \mathrm{f_u}(t) \approx \mathrm{f_u}^N(t) = \hat{\mathrm{f}}_{\mathrm{u}}\Phi(t)^{\intercal}, \tag{9}$$

where the coefficient vectors $\hat{\mathrm{x}} = [\hat{x}_1, \hat{x}_2, \cdots, \hat{x}_N]$ and $\hat{\mathrm{f}}_{\mathrm{u}} = [\hat{f}_{\mathrm{u}1}, \hat{f}_{\mathrm{u}2}, \cdots, \hat{f}_{\mathrm{u}N}]$ are both elements of the real vector space $\mathbb{R}^{n_b \times N}$. Within this (pseudo-)spectral framework, the equation of motion can be approximated [14] as:

$$\hat{\mathrm{v}} = (\hat{\mathrm{f}}_{\mathrm{e}} - \hat{\mathrm{f}}_{\mathrm{u}})\mathrm{G_o}, \tag{10}$$

where the coefficient vector $\hat{\mathrm{v}} = [v_1, v_2, \cdots, v_N]^{\intercal}$ represents the approximation of the system velocity $\mathrm{v}(t)$, and $\mathrm{G_o}$ denotes the force-to-velocity system *model*. Additionally, $\hat{\mathrm{f}}_{\mathrm{e}} = [\hat{f}_{\mathrm{e}1}, \hat{f}_{\mathrm{e}2}, \cdots, \hat{f}_{\mathrm{e}N}]^{\intercal}$, in Equation (10), represents the coefficient set $\hat{f}_{\mathrm{e}1}, \hat{f}_{\mathrm{e}2}, \cdots, \hat{f}_{\mathrm{e}N}$ that approximates the excitation force.

Taking into account the mathematical properties of the basis functions Φ_j [15], the objective function in Equation (7) can be approximated in the following manner:

$$E \approx J_N = \int_0^T \hat{\mathrm{f}}_{\mathrm{u}}\Phi(t)^{\intercal}\Phi(t)\hat{\mathrm{v}}^{\intercal} = -\frac{T}{2}\hat{\mathrm{f}}_{\mathrm{u}}\hat{\mathrm{v}}^{\intercal}, \tag{11}$$

This approximation converts the integral relationship expressed in Equation (7) into an algebraic mapping. By utilizing Equations (10) and (11), the objective function can be redefined as:

$$J_N = -(\hat{\mathrm{f}}_{\mathrm{e}} - \hat{\mathrm{f}}_{\mathrm{u}})\mathrm{G_o}\frac{T}{2}\hat{\mathrm{f}}_{\mathrm{u}}{}^{\intercal}, \tag{12}$$

In this way, the objective function is expressed in terms of the coefficient vectors $\hat{\mathrm{f}}_{\mathrm{u}}$, $\hat{\mathrm{f}}_{\mathrm{e}}$, and the force-to-velocity system model $\mathrm{G_o}$.

Within this context, the control problem for WEC systems can now be described as follows:

$$\begin{aligned} \hat{\mathrm{f}}_{\mathrm{u}}^{\star} \leftarrow \max_{\hat{\mathrm{f}}_{\mathrm{u}} \in \mathbb{R}^N} \quad & J_N \\ \text{subject to:} \quad & \mathcal{C}. \end{aligned} \tag{13}$$

The optimization problem presented in Eq. (13) is a quadratic optimization problem involving the variables $\hat{\mathrm{f}}_{\mathrm{u}}$. The problem is subject to a set of constraints $\mathcal{C}$ that arise from the physical limitations of the WEC system. In the specific application case discussed in Section V, the constraints $\mathcal{C}$ can be defined based on the maximum device displacement ($X_{\max}$), maximum PTO force ($F_{\max}$), or maximum velocity ($V_{\max}$).

To tackle the constrained optimization problem in Eq. (13), a collocation technique is employed, where

the constraints are enforced only at specific time points referred to as collocation points. By considering commonly used constraints such as $X_{\max}$ and $F_{\max}$, the set of constraints $\mathcal{C}$ in Equation (8) can be rewritten as a set of linear inequality constraints, as detailed in [16]. Finally, taking advantage of defined colocation points, general and standard multipurpose optimisation solvers (specifically QP-problem solvers) can be used to address the problem stated in Eq. (13).

IV. Control co-design problem

In this section, we introduce the formulation and solution approach for the CCD problem at hand. In general, the optimization problem for a WEC array control co-design scheme can be formulated as

$$\begin{aligned} \rho^{\text{opt}} \leftarrow \quad & \underset{\rho \in \mathbb{R}^N}{\text{Optimise}} && \Psi \\ & \text{subject to:} \quad \underset{\substack{\hat{\mathrm{f}}_{\mathrm{u}} \in \mathbb{R}^N \\ \mathcal{C}}}{\max} && J_N(\rho) \end{aligned} \tag{14}$$

where the optimization problem aims to minimize or maximize the objective function Ψ, with respect to the variable ρ, subject to the constraints considered by the spectral controller (as defined in Equation (13)). The specific form of the objective function Ψ depends on the particular specifications and requirements of the application. In this analysis, the objective function Ψ will capture the economic value of each array layout ρ, considering the optimised control actions for each device in the array.

A. Array objective function

As mentioned in the introduction, a crucial challenge in wave energy is the reduction of overall costs associated with WEC systems or WEC arrays[2]. In the literature, the levelized cost of energy (LCoE) is a prominent metric for assessing the economic viability of an energy source. Hence, this study introduces an optimization methodology to determine the optimal array layout using a metric derived from the LCoE. Typically, the LCoE is defined as follows:

$$\text{LCoE} = \frac{\text{CapEx} + \text{OpEx}}{\text{Energy production}}, \tag{15}$$

where the energy production is computed over the projected operational lifespan of the WEC array. It is worth noting that the units of LCoE are typically expressed as €/Wh. To provide some context, recent estimates for onshore and fixed-bottom offshore wind energy indicate LCoE values of 38$/MWh and 85$/MWh, respectively, as reported by [17].

As this is an initial study, several simplifying assumptions have been made to facilitate the analysis. The first simplification relates to the wave conditions at the location of the WEC array. To conduct a comprehensive assessment of the energy generated by the WEC array at a specific location, it would be necessary to consider range of different sea states. These sea states would be determined based on the probability distribution of their occurrence at the given location, often represented using a scatter diagram [18]. Consequently, if we (nominally) assume an operational lifespan of 20 years for the array, the analysis of energy production should be performed on an annual basis, taking into account potential variations in sea state intensity over time (e.g., increasing intensity and aggressiveness of sea states as the years progress, as illustrated in [19]). However, for the purpose of this analysis, as no specific deployment site is selected, we consider a single sea state (with multiple realizations for statistical consistency). It is important to note that when analyzing a single sea state, the results will remain unchanged regardless of whether the energy production is computed over the entire operational lifespan of the array or only over a short period of time. This is because the energy produced over the entire lifespan is determined by multiplying the energy produced for that particular sea state by the number of times that sea state occurs throughout the operational lifespan, which is consistent. As a result, the optimal array layout would be identical in both scenarios.

The costs of the WEC array, as indicated in Equation (15), can be categorized into capital and operational expenditure (CapEx and OpEx, respectively). In this study, the focus is solely on optimizing the layout of the WEC array, while keeping the devices themselves identical across all cases, which will (primarily) vary CapEx. Thus, for the present analysis, it will be assumed that OpEx is specified as a proportion of CapEx. As a result, OpEx does not impact the obtained results and is not taken into account in this study. However, it is worth noting that altering the array layout may affect the interactions between the devices, potentially influencing the behaviour of the WECs and, consequently, the maintenance requirements. Nonetheless, it is reasonable to assume that the associated costs resulting from these effects are relatively small compared to the CapEx.

The capital expenditure (CapEx) of the WEC arrays can be further broken down into the cost of the devices (DevEx), the cost of commissioning the devices (ComEx), and the cost of leasing the site (LeEx). Similarly, the cost of the devices can be divided into the cost of their individual components. Among such components, the mooring system of the array may vary depending on the layout being considered, thereby impacting the results since, in certain layouts, two WECs can share certain parts of the mooring system, such as the chain or the anchor. However, for the sake of simplicity and since the optimal layout is not affected by these components, they are not considered in this study. Therefore, the cost of the devices in the array can be defined as follows:

$$\text{DevEx} = n_{\text{an}} \mathrm{c}_{\text{an}} + \sum_{j=1}^{n_{\text{ch}}} \mathrm{L}_{\text{ch}_j} \mathrm{c}_{\text{ch}}, \tag{16}$$

where $n_{\text{an}} \in \mathbb{R}$ is the number of anchors to be installed, $\mathrm{c}_{\text{an}} \in \mathbb{R}$ the cost of each anchor, $n_{\text{ch}} \in \mathbb{R}$ the number

[2]Note that, from now on, the analysis will be focused on WEC arrays, since is the aim of this study, but could also be applied to single WECs.

of mooring lines in the array, $L_{ch_j} \in \mathbb{R}$ the length of the chain of the different mooring lines, and $c_{ch} \in \mathbb{R}$ the cost of the mooring chain per meter. It's important to note that when sharing the anchor, not only the cost of the anchor itself is saved, but also the cost of its installation, which can be considered as part of the commissioning cost (ComEx). In fact, in reality, since the cost of the anchor for a catenary mooring is proportional to the horizontal force, sharing an anchor would actually reduce its cost since the horizontal forces from the two moorings cancel each other. Thus, in the present analysis, the only commissioning cost considered is the cost associated with the installation of the anchor, as it is the only cost that varies depending on the layout; other commissioning costs are assumed to be the same regardless of the layout being considered. Hence, the anchor cost is defined as $c_{an} = c_{an_{mat}} + c_{an_{ins}}$, with $c_{an_{mat}} \in \mathbb{R}$ and $c_{an_{ins}} \in \mathbb{R}$ the material and installation costs, respectively. Finally, the site-leasing expenditure will vary depending on the area occupied by the array layout as

$$\text{LeEx} = c_{le} A_{ar}, \tag{17}$$

where $c_{le} \in \mathbb{R}$ denotes the cost of the area per square meter and A_{ar} the area occupied by the WEC array.

Thus, a new performance function, proportional to the LCoE of Equation (15), can be defined as

$$\text{LCoE}^* = \frac{n_{an} c_{an} + \sum_{j=1}^{n_{ch}} L_{ch_j} c_{ch} + c_{le} A_{ar}}{E}, \tag{18}$$

with the generated energy E as in Equation (7).

B. Problem Solution

As introduced in [20], the problem stated in Equation (14) is usually approached using different methods:

- **Control-inspired** paradigms leverage engineering knowledge of dynamics and control principles. They propose new control solutions based on low-fidelity models and control engineering tools.
- **Co-optimisation** techniques employ mathematical methodologies with nonlinear models and optimisation theory. They consider the cost function of the plant architecture, dynamics, and controller design, allowing changes in the structures during the optimization process.
- **Co-simulation** methods use high/mixed-fidelity dynamic models in iterative simulations. They incorporate optimization algorithms, data-based models, and machine learning techniques. Co-simulation is advantageous in handling the complexity of CCD problems, offering integration of models, iterative design refinement, and flexibility in exploring design options.

In essence, as concluded in [20], co-simulation is an effective methodology for finding optimal solutions in CCD problems, enabling comprehensive system dynamic analysis, efficient exploration of design options, and reduced design cycle time. It can integrate multiscale and multiphysics models, incorporate optimization algorithms and data-driven techniques, and provide a modular design approach. For further details on CCD solution methodologies, refer to [20].

In this study, we use a co-simulation approach to solve the CCD problem stated in Equation (14). Ideally, this co-simulation approach would be combined with an optimal point search algorithm, such as linear or binary search methods. Nevertheless, when examining and modifying WEC array layout designs within a CCD loop, it becomes necessary to recalculate hydrodynamic coefficients, in order to incorporate the updated geometry. This process involves running boundary element method (BEM) software for each iteration. Consequently, even for WEC arrays with relatively straightforward layout configurations, the computational requirements of the CCD optimisation loop can quickly become overwhelming and impractical. However, to simplify the problem and present results for all array layouts, we employ an exhaustive search procedure. Such a parametric study involves computing the results for all possible WEC array layouts to determine which case minimizes the objective function proposed in Section IV-A, and carries the advantage that full information on the search space is returned.

V. Illustrative example

In this section, we present an illustrative example to highlight the advantages of the CCD method introduced in this paper. By applying this methodology to a specific case study, we aim to demonstrate the benefits and potential enhancements that can be achieved by integrating advanced control strategies with system design, rather than relying on simple passive controllers. Through this example, we emphasize the significance of incorporating control considerations from the early stages of system development, leading to improved performance and optimized outcomes in practical applications.

A. Sea state

As mentioned in Section IV, in this study, a simplified approach is taken by considering a single panchromatic sea state with three different wave directions (0, 45, and 90 degrees, see Fig. 1), whereas a more comprehensive analysis would involve the use of a scatter diagram to capture the statistical characteristics of the sea conditions at a specific wave energy site [18]. The waves are synthesized using filtered white noise [21] based on a JONSWAP spectrum [22]. The selected parameters for the synthesized sea state are a significant wave height of $H_s = 2.5$ m, a peak period of $T_p = 10$ s, and a steepness factor of $\gamma = 3.3$. To ensure statistical consistency, 10 realizations of the sea state are considered. Each simulation is conducted over a duration of 300 s, which is equivalent to 30 times the peak period of the chosen sea state. Finally, the water depth is assumed to be 100m.

B. WEC array

The WEC array under consideration consists of three identical devices arranged in a linear configuration, as

depicted in Fig. 1. The devices are cylindrical heaving WECs with a diameter of $\varnothing = 10$m and a draft of 10m. It is important to note that assuming the WECs move solely in the heave direction is a strong simplifying assumption, considering that the optimization algorithm incorporates the mooring system in the objective function, since contemplating other degrees of freedom (such as surge and sway) would significantly impact the mooring configuration selection. Moreover, when accounting for surge and sway motions, the selection of a correct minimum inter-device distance becomes crucial to avoid collisions. However, for the purpose of this study, which aims to demonstrate the proposed methodology in a straightforward manner, we assume that the WECs only move in the heave direction. Additionally, it is assumed that the effect of the moorings on the system follows the same stiffness and damping characteristics discussed in Section II, regardless of the specific mooring configuration (e.g., individual mooring chains or shared chains with neighbouring devices).

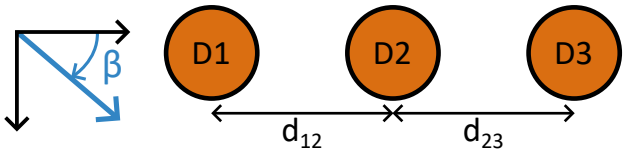

Fig. 1. Sketch of the considered WEC array layout with β the direction of the waves.

Fig. 1 illustrates the WEC array layout, where the three devices composing the array are denoted as D1, D2, and D3. The key aspect that will be varied in the array configurations is the inter-device distance between D1 and D2 (d12) and between D2 and D3 (d23). These inter-device distances are expressed as multiples of the device diameter ($\varnothing$). In this study, the range of inter-device distances considered spans from $2\varnothing$ to $28\varnothing$, corresponding to distances between 20m and 280m. Additionally, the three wave directions considered allow showing how the results vary when the wavefront hit the three devices at the same time ($\beta = 90°$), when the devices are one behind another in the direction of the waves ($\beta = 0°$), and the middle scenario ($\beta = 45°$).

C. Mooring cost

In accordance with Section IV-A, the mooring system costs are the only costs that vary depending on the array layout. Consequently, three different scenarios, as illustrated in Fig. 2, are considered based on the inter-device distance:

- If the inter-device distance is larger than d_s, the device will be moored separately and, hence, will have two independent mooring chains (of length L_i) and two anchors;
- if the inter-device distance is d_s, the two devices will share the anchor, but will have their own separate mooring chain;
- if the inter-device distance is smaller than d_s, the two devices will be connected to each other by means of a shared mooring chain (of a length L_s, which depends on the inter-device distance) and will not have an anchor.

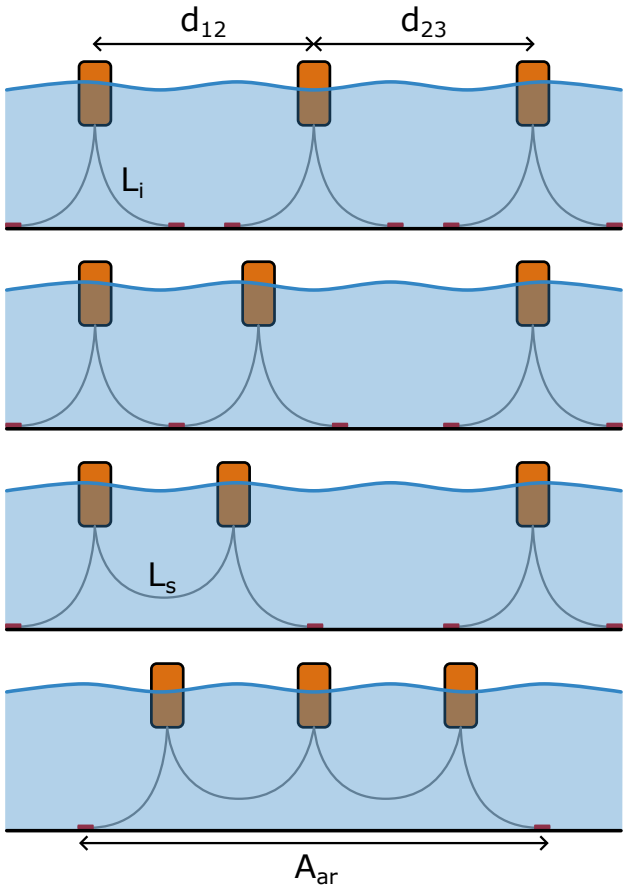

Fig. 2. Sketch of the different mooring configurations.

Fig. 2 depicts various mooring configurations, ranging from three independent mooring systems (top figure) to three bodies sharing a common mooring (bottom figure). The array area, denoted A_{ar}, is indicated in the figure and is used to compute the site-leasing expenditure according to Equation (17).

The costs of the anchors (c_{an}) and chain (c_{ch}) are determined based on the cost estimates provided in [23], which are presented in Table I. One could notice that Table I shows the costs as a function of the maximum steady state anchor forces and line tensions. In this study, a value of 10^4 kN is used for these forces. However, it is important to note that, in a more detailed analysis, the mooring system should be optimised so that such force takes into account potential extreme events that may occur at the site, among other possible forces.

TABLE I
COST OF THE MOORING COMPONENTS. FROM [23].

	Material	Installation
Anchor cost	€ 93/kN/anchor	€ 4600/kN/anchor
Chain cost	€ 0.39/kN/m	-

To account for the varying lengths of the chains and, hence, calculate their cost following the unit costs

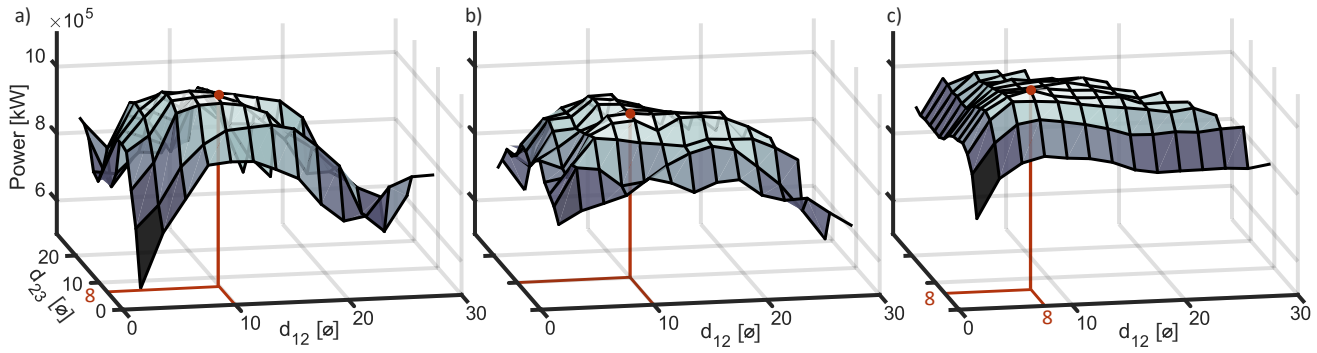

Fig. 5. Absorbed power from the waves for all the array layouts considered, with wave direction (a) $\beta = 0°$, (b) $\beta = 45°$, and (c) $\beta = 90°$, and the maximum value highlighted in red.

provided in Table I, the shape of the moorings is modelled using the catenary equation as

$$y_{\mathrm{m}}(x_{\mathrm{m}}, d_{\mathrm{id}}) = a_{\mathrm{m}}(d_{\mathrm{id}}) \cosh\left(\frac{x_{\mathrm{m}}}{a_{\mathrm{m}}(d_{\mathrm{id}})}\right), \qquad (19)$$

with $a_{\mathrm{m}}(d_{\mathrm{id}})$ a constant (that depends on the inter-device distance) to shape the catenary curve. The mooring system for different configurations is depicted in Fig. 3, based on the model presented in Equation (19). The figure illustrates the mooring shape with a black line for the scenario where the inter-device distance is $\mathrm{d_s}$, indicating that both devices share the anchor but have independent mooring chains. Additionally, grey lines represent different cases of inter-device distance, ranging from $2\varnothing$ to $10\varnothing$, where two devices share the mooring line. It is worth noting that, for the case study analyzed in this study, $\mathrm{d_s}$ is set to $12\varnothing$, as shown in Fig. 3. To provide some context, the mooring chain lengths shown in Fig. 3 range from approximately 250 meters for the black line to 125 meters for the lightest grey line, corresponding to (approximately) € $9.7 \cdot 10^5$ and € $4.8 \cdot 10^5$, respectively.

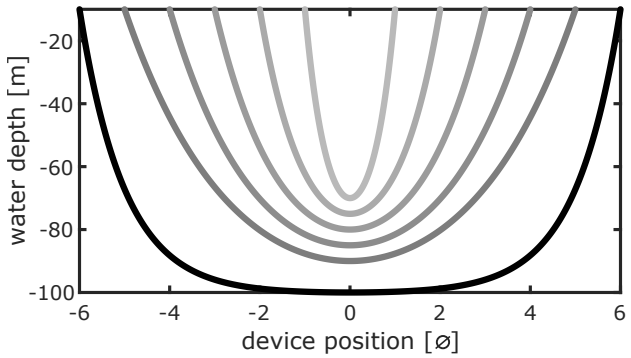

Fig. 3. Considered mooring lines shape depending on the inter-device distance.

The leasing cost of the site per square meter is estimated following the methodology introduced in [24], where it is assumed to be approximately one-third of the cost of the complete mooring system. Therefore, for a device with an independent mooring system, the leasing cost per linear meter can be calculated as follows:

$$\mathrm{c_{le}} = \frac{2(\mathrm{c_{an}} + \mathrm{L_i c_{ch}})}{3\mathrm{d_{le}}}, \qquad (20)$$

with $\mathrm{d_{le}}$ the distance between anchors for an independent mooring configuration which, as shown in Fig. 3, is $\mathrm{d_{le}} = 2 \cdot 6\varnothing = 120$ m. Thus, the leasing cost per linear meter is $\mathrm{c_{le}} \approx 1.1 \cdot 10^4$ €/m and the total cost will depend on the total length of the array ($\mathrm{A_{ar}}$, as shown in Fig. 2).

Finally, Fig. 4 illustrates the total mooring cost for all the considered array configurations. It should be noted that the results are presented as a function of $\mathrm{d_{12}}$ and $\mathrm{d_{23}}$, and there is symmetry along the diagonal axis. This symmetry arises from the fact that, for geometrically non-symmetric array layouts, the costs and obtained results are the same for two layouts if they are symmetric pairs (i.e. if $\mathrm{d_{12}}$ in one layout is equal to $\mathrm{d_{23}}$ in another layout, and vice versa). In Fig. 4, a clear step in the cost can be appreciated at $\mathrm{d_{id}} = 10\ \varnothing$, corresponding to the chosen $\mathrm{d_s}$. This step signifies the need for additional anchors to be installed, as the WECs are too far apart to share a mooring chain.

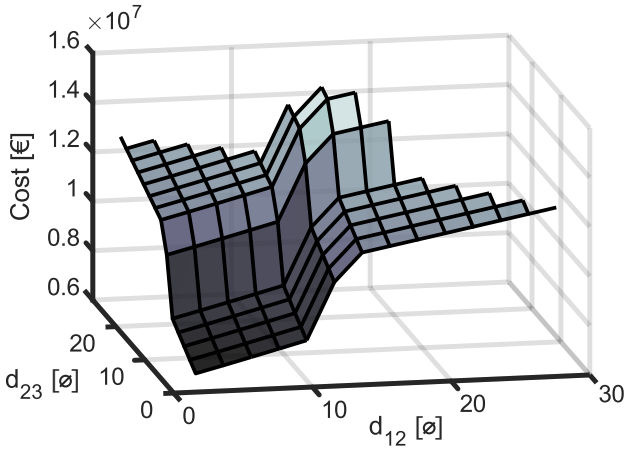

Fig. 4. Mooring systems costs for all the array layouts considered.

D. CCD results

This section discusses the results obtained from the CCD algorithm. Fig. 5 illustrates the power absorbed by the different array layouts for the three wave directions considered. Firstly, it should be noted that, as expected, the power obtained in all the cases is in the same order of magnitude[3], regardless of the layout or

[3]Note that the three figures of Fig. 5 share the same axis discretisation, defined for Fig. 5(a).

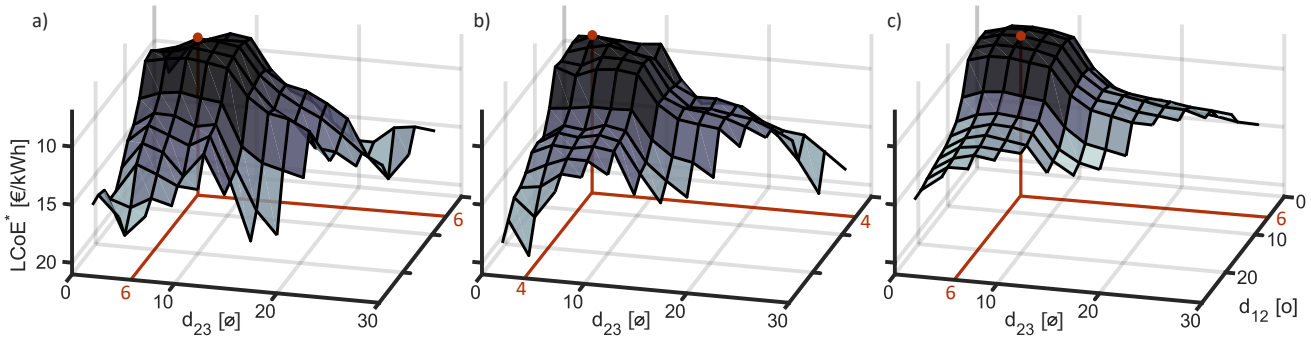

Fig. 7. Obtained LCoE* values for all the array layouts considered, with wave direction (a) $\beta = 0°$, (b) $\beta = 45°$, and (c) $\beta = 90°$, and the minimum value highlighted in red. Note that the z-axis is inverted to better appreciate the shape of the function.

wave direction. The figures show how the array layout providing the maximum power differs depending on the wave direction, although it is similar for all the cases (between 8 ⌀and 10 ⌀). It is shown that, apart from obtaining the highest powers, the case with the waves coming at 90° is the least influenced by the interactions between the devices (the difference between the lowest and highest point is the smallest); while, on the contrary, for $\beta = 0°$ the effect of the interactions vary more severely from one layout to another, hence obtaining a larger variation on the generated power. Note that such effects make sense since, for $\beta = 90°$, the interactions are mainly due to radiated waves, while, for $\beta = 0°$, the interactions are due to both radiated and diffracted waves.

Fig. 5(c) shows that, for inter-device distances larger than approximately 6 ⌀, the absorbed power exhibits a slight decrease but not overly significant, and converges to a specific value. This makes sense since, as d_{12} and d_{23} increase, the WECs in the array become more separated, resulting in reduced hydrodynamic interactions. Thus, if the inter-device distance is sufficiently large, the absorbed power in the array should (theoretically) converge to three times the power generated by a single isolated WEC. However, it should be noted that such an effect is not that easy to see in Fig. 5(a), possibly due to the larger amount of interactions, hence requiring larger inter-device distances.

To identify the best array layout for all the wave directions considered, the results shown in Fig. 5 are averaged, as shown in Fig. 6. The power is observed to be significantly influenced by the inter-device distance, particularly for smaller distances where the power decreases substantially. In this case, the array layout obtaining the largest power is that with the inter-device distance of 8 ⌀.

After calculating the cost and power absorption for each layout, the LCoE* can be computed using Equation (15). Fig. 7 displays the LCoE* values for the different array layouts and wave directions considered in this study. As expected, since the cost is the same regardless of the wave direction and considering the generated power shown in Fig. 5, the minimum LCoE* value differs for the three wave directions, although they all are in the same range.

By averaging the LCoE* values for all the wave directions shown in Fig. 7, the results shown in Fig. 8

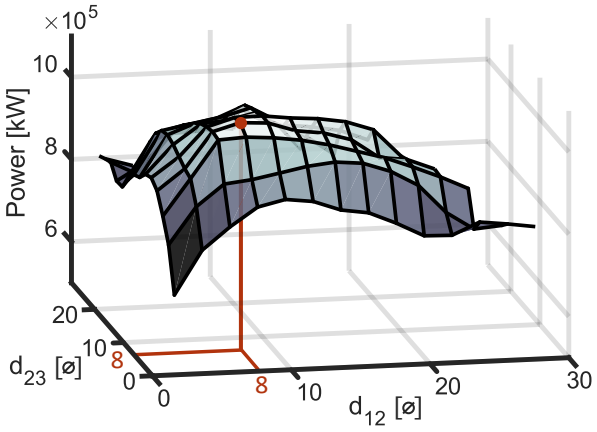

Fig. 6. Absorbed power from the waves for all the array layouts considered averaged over the wave directions, with the maximum value highlighted in red.

are obtained. Notably, the optimal array layout, based on the specified conditions, corresponds to a symmetric layout with an inter-device distance of $d_{12} = d_{23} = 6$ ⌀. This optimal layout aligns with the expected results observed in Figures 4 and 6, further reinforcing the effectiveness of the proposed optimization methodology.

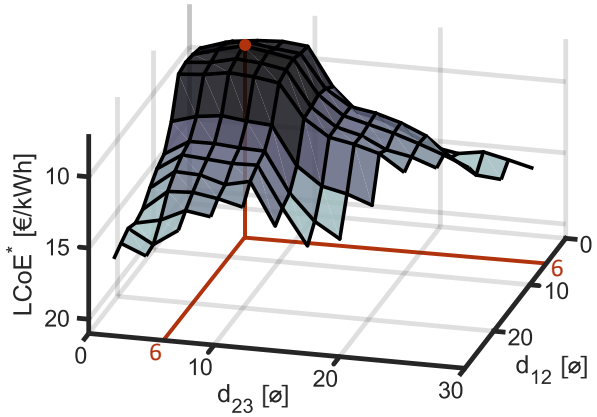

Fig. 8. Obtained LCoE* values for all the array layouts considered averaged over the three wave directions, with the minimum value highlighted in red.

It is important to clarify that the magnitudes of the results obtained in this study are not meant to be interpreted as fully realistic or meaningful in absolute terms. They are displayed solely for the purpose of comparing the outcomes with those obtained using a

simple controller (shown in Section V-E). Additionally, the costs considered in the analysis may not accurately reflect real-world scenarios, and the optimal layout obtained could vary if different specifications are taken into account. However, it is crucial to emphasize that the objective of this section is not to present a real case study, but rather to demonstrate, by means of an illustrative example, the optimization methodology proposed in this paper.

E. Results with passive controller

In this section, a similar analysis to the previous section is conducted, but with the inclusion of a simple proportional controller based on the device velocity. The damping coefficient of the controller is optimized for each inter-device distance and wave direction. Note that, for the sake of conciseness, only the results averaged over the three wave directions are shown in this subsection. Fig. 9 illustrates the power absorption of the different array layouts for the given sea state, similar to Fig. 6. In this case, the maximum power absorption is achieved with the symmetric array layout featuring d_{12} =d_{23} = 8 ⌀. However, the differences in power absorption between the minimum and maximum values are much less significant compared to Fig. 6. Also, one could notice that the power absorbed with this controller is significantly less than that obtained with the spectral control (around 7 times less).

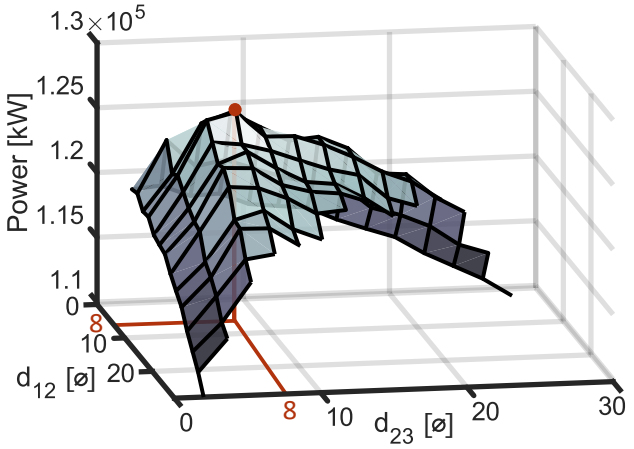

Fig. 9. Absorbed power from the waves for all the array layouts, considering a simple proportional controller, averaged over the three wave directions.

The optimisation results obtained for the proportional controller are illustrated in Fig. 10, where the d12 =d23 = 2 ⌀configuration is shown to yield the highest LCoE* value, coinciding with the least expensive array layout depicted in Fig. 4. In fact, it is evident that the surface plot in Fig. 10 exhibits an inverse relationship with the surface plot in Fig. 4. This outcome arises from the minimal differences in absorbed power among all the inter-device distances, as evidenced in Fig. 9. Consequently, the LCoE primarily depends on the inverse of the cost factor rather than the absorbed power. It should be noted that Fig. 10 suggests an optimal inter-device distance of 0 ⌀, reflecting the most cost-effective mooring configuration. However, it is essential to recognise that such a scenario is not physically feasible. The present study did not consider the minimum inter-device distance required to avoid over-positioning (or even collisions between) the devices, which must be taken into account for practical implementation.

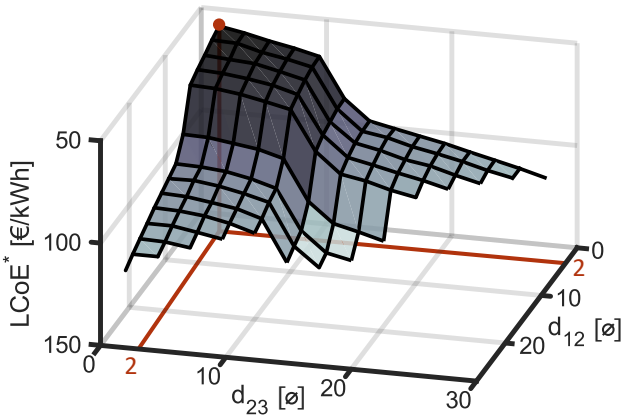

Fig. 10. Obtained LCoE* values for all the array layouts, with the maximum value highlighted in red, considering a simple proportional controller, averaged over the three wave directions.

Lastly, it is important to emphasize that, as mentioned before, if the proposed CCD methodology is not employed and the array layout optimization is performed using a simple controller, followed by the implementation of an advanced control strategy on the final layout, the results may not be optimal. In the current example, if the optimal layout obtained from the optimization with the simple controller (d_{12} =d_{23} = 2 ⌀) is used with the optimal controller, the outcomes will be suboptimal. This can be observed in Fig. 8, where the LCoE* values for this combined approach are lower compared to the results obtained using the CCD methodology. Therefore, it underscores the significance of integrating advanced control strategies during the layout optimization process to achieve optimal outcomes.

VI. Conclusion

This study introduces a novel control co-design (CCD) methodology for optimizing the layout of a wave energy converter (WEC) array, taking into account the economic factor of considering different mooring system configurations. The results highlight the influence of controller selection within the optimisation process on the optimal array layout, emphasizing the importance of incorporating advanced control techniques at early design stages. The CCD methodology demonstrates its effectiveness in achieving optimized WEC array layouts that balance power absorption and component cost considerations.

References

[1] J. V. Ringwood, "Wave energy control: status and perspectives 2020," *IFAC-PapersOnLine*, vol. 53, no. 2, pp. 12 271–12 282, 2020, 21st IFAC World Congress.

[2] A. Mérigaud and J. V. Ringwood, "Improving the computational performance of nonlinear pseudospectral control of wave energy converters," *IEEE Transactions on Sustainable Energy*, vol. 9, no. 3, pp. 1419–1426, 2018.

[3] R. G. Coe, G. Bacelli, S. Olson, V. S. Neary, and M. B. R. Topper, "Initial conceptual demonstration of control co-design for WEC optimization," *Journal of Ocean Engineering and Marine Energy*, vol. 6, no. 4, pp. 441–449, 2020.
[4] Y. Peña-Sanchez, D. García-Violini, and J. V. Ringwood, "Control co-design of power take-off parameters for wave energy systems," *IFAC-PapersOnLine*, vol. 55, no. 27, pp. 311–316, 2022.
[5] G. Bacelli, J. V. Ringwood, and J.-C. Gilloteaux, "A control system for a self-reacting point absorber wave energy converter subject to constraints," *IFAC Proceedings Volumes*, vol. 44, no. 1, pp. 11 387–11 392, 2011.
[6] P. B. Garcia-Rosa, G. Bacelli, and J. V. Ringwood, "Control-informed optimal array layout for wave farms," *IEEE Transactions on Sustainable Energy*, vol. 6, no. 2, pp. 575–582, 2015.
[7] T. F. Ogilvie, "Recent progress toward the understanding and prediction of ship motions," in *5th Symposium on Naval Hydrodynamics*, vol. 1. Bergen, Norway, 1964, pp. 2–5.
[8] J. Falnes, *Ocean Waves and Oscillating Systems: Linear Interactions Including Wave-Energy Extraction*. Cambridge Univ. Press, 2002.
[9] D. García-Violini, Y. Peña-Sanchez, N. Faedo, and J. V. Ringwood, "An energy-maximising linear time invariant controller (LiTe-Con) for wave energy devices," *IEEE Transactions on Sustainable Energy*, vol. 11, no. 4, pp. 2713–2721, 2020.
[10] LHEEA, NEMOH-Presentation, "Laboratoire de Recherche en Hydrodynamique Énergetique et Environnement Atmospherique," https://goo.gl/yX8nFu, 2017, [Online accessed 1-Aug-2019].
[11] N. Faedo, Y. Peña-Sanchez, and J. V. Ringwood, "Finite-order hydrodynamic model determination for wave energy applications using moment-matching," *Ocean Engineering*, vol. 163, pp. 251–263, 2018.
[12] WAMIT, "Wamit," https://www.wamit.com, 202023, online accessed 1-Jun-2023.
[13] N. Faedo, S. Olaya, and J. V. Ringwood, "Optimal control, MPC and MPC-like algorithms for wave energy systems: An overview," *IFAC Journal of Systems and Control*, vol. 1, pp. 37–56, 2017.
[14] D. Garcia-Violini and J. V. Ringwood, "Energy maximising robust control for spectral and pseudospectral methods with application to wave energy systems," *International Journal of Control*, vol. 94, no. 4, pp. 1102–1113, 2021.
[15] D. García-Violini, M. Farajvand, C. Windt, V. Grazioso, and J. V. Ringwood, "Passivity considerations in robust spectral-based controllers for wave energy converters," in *2021 XIX Workshop on Information Processing and Control (RPIC)*. IEEE, 2021, pp. 1–6.
[16] G. Bacelli and J. V. Ringwood, "Numerical optimal control of wave energy converters," *IEEE Transactions on Sustainable Energy*, vol. 6, no. 2, pp. 294–302, 2015.
[17] T. Stehly, P. Beiter, and P. Duffy, "2019 cost of wind energy review," NREL, USA, Tech. Rep., 12 2020.
[18] S. Barstow, G. Mørk, D. Mollison, and J. Cruz, "The wave energy resource," in *Ocean Wave Energy*. Springer, 2008, pp. 93–132.
[19] A. Ulazia, M. Penalba, G. Ibarra-Berastegui, J. Ringwood, and J. Saénz, "Wave energy trends over the Bay of Biscay and the consequences for wave energy converters," *Energy*, vol. 141, pp. 624–634, 2017.
[20] M. Garcia-Sanz, "Control co-design: An engineering game changer," *Advanced Control for Applications: Engineering and Industrial Systems*, vol. 1, no. 1, p. e18, 2019.
[21] M. Tucker, P. G. Challenor, and D. Carter, "Numerical simulation of a random sea: a common error and its effect upon wave group statistics," *Applied ocean research*, vol. 6, no. 2, pp. 118–122, 1984.
[22] K. Hasselmann, "Measurements of wind wave growth and swell decay during the Joint North Sea Wave Project (JONSWAP)," *Deutches Hydrographisches Institut*, vol. 8, p. 95, 1973.
[23] C. Fontana, "A multiline anchor concept for floating offshore wind turbines," Ph.D. dissertation, 2019.
[24] I. Touzon, V. Nava, B. de Miguel, and V. Petuya, "A comparison of numerical approaches for the design of mooring systems for wave energy converters," *Journal of Marine Science and Engineering*, vol. 8, no. 7, p. 523, 2020.